1-1-2003

Output Feedback Force Control for a Parallel Turning Operation

Raghusimha Sudhakara

Robert G. Landers
Missouri University of Science and Technology, landersr@mst.edu

Recommended Citation

R. Sudhakara and R. G. Landers, "Output Feedback Force Control for a Parallel Turning Operation," *Proceedings of the 2003 American Control Conference, 2003*, Institute of Electrical and Electronics Engineers (IEEE), Jan 2003.
The definitive version is available at https://doi.org/10.1109/ACC.2003.1243468

Output Feedback Force Control for a Parallel Turning Operation

Raghusimha Sudhakara
Performance Consulting Services
Montrose, Colorado 81401
rsudhakara@pcs-mail.com

Robert G. Landers
University of Missouri at Rolla, Department MAEEM
Rolla, Missouri 65409
landersr@umr.edu

ABSTRACT – Parallel machine tools (i.e., machine tools capable of cutting a part with multiple tools simultaneously but independently) are being utilized more and more to increase operation productivity, decrease setups, and reduce floor space. Process control is the utilization of real-time process sensor information to automatically adjust process parameters (e.g., feed, spindle speed) to increase operation productivity and quality. To date, however these two technologies have not been combined. This paper describes the design of an output feedback controller for a parallel turning operation that accounts for the inherent nonlinearities in the force process. An analysis of the process equilibriums explains the system stability behavior for different design specifications and the reverse trajectory method is used to numerically determine the exact stability boundary. Effects of saturation on stability are also analyzed and from this sufficient conditions for global stability are obtained.

INTRODUCTION – In manufacturing there is a constant need for productivity and quality improvements. To realize these improvements, there have been two developments in the machining community: process control and parallel (i.e., simultaneous) machine tools. An enormous amount of research in process control has focused on the area of machining force regulation. Various force control approaches have been developed for different processes such as turning, milling, etc., resulting in significant productivity gains. Most force control strategies utilize adaptive control techniques (e.g., [1]). Others include direct model-based methods (e.g., [2]) and robust (e.g., [3]) techniques. Parallel machine tools (and parallel machining) have emerged as a new alternative to conventional machine tools. Levin and Dutta [4] and Yip-Hoi and Dutta [5] have discussed these from a process planning perspective. Force controllers for these machine tools have not been investigated or developed thus far. In this paper, a stepped part turned by two single point cutting tools is considered. Figure 1 provides a schematic illustrating the process.

In this paper, an output feedback based force controller is developed for a parallel turning operation utilizing two tools. A static force feed model is used to characterize the cutting forces. A first order servo model is used for the feed dynamics and a linear output feedback law is implemented. Sufficient conditions are obtained for control gains to ensure global asymptotic stability of the closed-loop system. Simulations and phase plots are used to validate the analysis. Finally, the controller is investigated for robustness to parameter uncertainties.

FORCE PROCESS MODEL – In this section a force process model is presented for a parallel lathe with two tools. Machining force processes are nonlinear and depend on a number of parameters. The model used in this paper couples a static force process with a first-order servomechanism system. The cutting force model for each tool is

$$F_i = K_i d_i^{\beta_i} V_i^{\gamma_i} f_i^{\alpha_i} = \bar{K}_i f_i^{\alpha_i} \qquad i = 1,2 \tag{1}$$

The transfer function between the actual and commanded feed is

$$\frac{f_i}{f_{c_i}} = \frac{1}{\tau_i s + 1} \qquad i = 1,2 \tag{2}$$

Combining equations (1) and (2)

$$\tau_i \dot{F}_i + F_i = \bar{K}_i f_{c_i}^{\alpha_i} \qquad i = 1,2 \tag{3}$$

The part and tool structures are assumed to be rigid and, thus, there is no direct coupling between the two force processes. Typically, maximum metal removal rates are achieved when operating at the machine tool spindle's maximum continuous power; therefore, the machining force controller designed below will regulate the spindle power at this maximum value. In this paper, the spindle power is divided equally between the two tools. Corresponding to the maximum power, reference forces are computed for a given spindle speed. The maximum spindle power is

$$P_{\max} = \sum_{i=1}^{2} V_i F_{r_i} \tag{4}$$

where

$$F_{r_i} = \frac{1}{2}\frac{P_{\max}}{V_i} \qquad i = 1,2 \tag{5}$$

The nominal feeds are

$$f_{n_i} = \left(\frac{F_{r_i}}{K_i d_i^{\beta_i} V_i^{\gamma_i}}\right)^{\frac{1}{\alpha_i}} \qquad i = 1,2 \tag{6}$$

Equation (3) is linearized about the reference forces and feeds. The linearized model, in terms of perturbed forces, feeds, and power is given by

$$\begin{bmatrix} \Delta\dot{F}_1 \\ \Delta\dot{F}_2 \end{bmatrix} = \begin{bmatrix} -\frac{1}{\tau_1} & 0 \\ 0 & -\frac{1}{\tau_2} \end{bmatrix} \begin{bmatrix} \Delta F_1 \\ \Delta F_2 \end{bmatrix} + \begin{bmatrix} \frac{\bar{K}_{1a}}{\tau_1} & 0 \\ 0 & \frac{\bar{K}_{2a}}{\tau_2} \end{bmatrix} \begin{bmatrix} \Delta f_{c_1} \\ \Delta f_{c_2} \end{bmatrix} \tag{7a}$$

$$\Delta P = \begin{bmatrix} V_1 & V_2 \end{bmatrix} \begin{bmatrix} \Delta F_1 \\ \Delta F_2 \end{bmatrix} = C \begin{bmatrix} \Delta F_1 \\ \Delta F_2 \end{bmatrix} \tag{7b}$$

where $\bar{K}_{ia} = K_i \alpha_i f_{n_i}^{(\alpha_i - 1)}$, $\Delta F_i = F_i - F_{r_i}$, and $\Delta f_{c_i} = f_{c_i} - f_{n_i}$, $i = 1,2$ and $\Delta P = P - P_{\max}$.

Since the origin is an equilibrium of the linearized system, the control problem is reduced to a regulation problem. Expressing the original nonlinear equations in terms of the perturbed forces and feeds

$$\Delta\dot{F}_i = -\frac{\Delta F_i + F_{r_i}}{\tau_i} + \frac{\bar{K}_i}{\tau_i}\left[\Delta f_{c_i} + f_{n_i}\right]^{\alpha_i} \qquad i = 1,2 \tag{8}$$

The origin is clearly an equilibrium of the original nonlinear system as well. From equation (7a) it is evident that the eigenvalues of the Jacobian are negative and real and, thus, the system is Hurwitz indicating that the equilibrium of the nonlinear system is a stable node.

Saturation constraints are imposed on the commanded feeds. The lower saturation limits are zero since it is not desirable for the tool

to disengage from the part. Upper saturation limits are also imposed due to process or machine tool constraints.

CONTROLLER DESIGN – This section describes the design procedure for the output feedback controller. The design is based on the linearized system model given in equations (7a) and (7b). The linear feedback control law is

$$\Delta\tilde{f}_c = -H\Delta P = -HC\Delta\tilde{F} \tag{9}$$

Where $\Delta\tilde{f}_c^T = \begin{bmatrix}\Delta f_{c_1} & \Delta f_{c_2}\end{bmatrix}$ and $\Delta\tilde{F}^T = \begin{bmatrix}\Delta F_1 & \Delta F_2\end{bmatrix}$. This results in the closed loop system

$$\Delta\dot{\tilde{F}} = (A - BHC)\Delta\tilde{F} = A_{cl}\Delta\tilde{F} \tag{10}$$

with the eigenvalues of the matrix A_{cl} being at the locations required by the design specifications. A solution for H to place poles of the system almost arbitrarily exists if the system is completely controllable. The controllability matrix is

$$Q = \begin{bmatrix} \frac{\bar{K}_{1a}}{\tau_1} & 0 & -\frac{\bar{K}_{1a}}{\tau_1^2} & 0 \\ 0 & \frac{\bar{K}_{2a}}{\tau_2} & 0 & -\frac{\bar{K}_{2a}}{\tau_2^2} \end{bmatrix} \tag{11}$$

which has full rank. Thus, the closed loop poles can arbitrarily be placed almost anywhere in the complex plane [6].

The following design algorithm is used to obtain the output feedback controller.

Step 1: Choose the desired eigenspectrum based on the design specifications. If m_1 and m_2 are the design time constants, then the required eigenspectrum is $\lambda = \begin{bmatrix}-1/m_1 & -1/m_2\end{bmatrix}$.

Step 2: Design a full state feedback controller [7] such that $\Delta\tilde{f}_c = -K\Delta\tilde{F}$. One such gain matrix for a full state feedback controller is given by

$$K = \begin{bmatrix} -\frac{1}{\bar{K}_{1a}} & -\frac{\tau_1}{\bar{K}_{1a}} \\ \frac{\tau_2}{m_1 m_2 \bar{K}_{2a}} & \frac{\tau_2(m_1+m_2) - m_1 m_2}{m_1 m_2 \bar{K}_{2a}} \end{bmatrix} \tag{12}$$

Step 3: Obtain the output feedback controller gain vector from the full state feedback gain matrix [8]. Comparing the closed–loop matrix A_{cl} in equation (10) with that in the full state feedback design, the following relationship is established

$$K = HC \tag{13}$$

The vector H is obtained by post multiplying C^g on both sides

$$H = KC^g \tag{14}$$

where C^g is the pseudo inverse of the matrix C.

Theorem 1 [8]: A necessary and sufficient condition for all of the poles described by equation (10) to be arbitrarily assigned by using constant output feedback is that one of the set of state feedback matrices K, which achieves the same pole placement, and one of the pseudo–inverses of C satisfy the consistence relationship $KC^gC = K$, where C^g is given by $(CC^g)C = C$.

The vector H is determined analytically in terms of the system parameters and is

$$H = KC^g = \begin{bmatrix} -\frac{V_1 + \tau_1 V_2}{\bar{K}_{1a}(V_1^2 + V_2^2)} \\ \frac{\tau_2 V_1 + \tau_2 V_2 (m_1 + m_2) - m_1 m_2 V_2}{\bar{K}_{2a}(V_1^2 + V_2^2)} \end{bmatrix} \tag{15}$$

This gain matrix satisfies the conditions of Theorem (1). Since the matrix H places the poles in the desired locations exactly, the closed loop system matrix is Hurwitz and consequently, the linearized closed–loop system is stable.

FORCE PROCESS MODEL AND SIMULATION PARAMETERS – Simulation studies will subsequently be performed to analyze the controller performance. The cutting force data for a steel part and a coated carbide insert are used to obtain the parameters for the nonlinear force process model [9]. The least squares method is used and the correlation coefficient is 0.96, indicating a very good fit. The list of the various parameters used in the subsequent simulations is given in Table 1. The fourth order Runge–Kutta numerical integration method is used and a sample period of 0.004 *s* is chosen. Saturation constraints as discussed earlier are incorporated into the simulations where the maximum commanded feeds are 1.5 *mm*.

STABILITY ANALYSIS – In this section the stability of the closed–loop nonlinear system is analyzed. The closed–loop system dynamics are found by inserting the control law given by equation (9) into the open loop nonlinear system given by equation (8). Combining these equations results in

$$\Delta\dot{F}_1 = -\frac{(\Delta F_1 + F_{r_1})}{\tau_1} + \frac{\bar{K}_1}{\tau_1}\left[-h_1 V_1 \Delta F_1 - h_1 V_2 \Delta F_2 + f_{n_1}\right]^{\alpha_1} \tag{16}$$

$$\Delta\dot{F}_2 = -\frac{(\Delta F_2 + F_{r_2})}{\tau_2} + \frac{\bar{K}_2}{\tau_2}\left[-h_2 V_1 \Delta F_1 - h_2 V_2 \Delta F_2 + f_{n_2}\right]^{\alpha_2}$$

In terms of the actual forces, the nonlinear equations are

$$\dot{F}_1 = -\frac{F_1}{\tau_1} + \frac{\bar{K}_1}{\tau_1}\left[-h_1 V_1 (F_1 - F_{r_1}) - h_1 V_2 (F_2 - F_{r_2}) + f_{n_1}\right]^{\alpha_1} \tag{17a}$$

$$\dot{F}_2 = -\frac{F_2}{\tau_2} + \frac{\bar{K}_2}{\tau_2}\left[-h_2 V_1 (F_1 - F_{r_1}) - h_2 V_2 (F_2 - F_{r_2}) + f_{n_2}\right]^{\alpha_2} \tag{17b}$$

One equilibrium point of the perturbed system is the origin as discussed before. The eigenvalues of the Jacobian of the nonlinear system given by equation (16) are located in the negative half plane, their exact locations depending on the desired closed–loop time constants.

Theorem 2 [10]: The equilibrium point at the origin of equation (10) is stable if and only if all eigenvalues of the Jacobian satisfy $Re(\lambda_i) \le 0$ and every eigenvalue with $Re(\lambda_i) = 0$ has an associated Jordan block of order one. The equilibrium point is asymptotically stable if and only if all the eigenvalues of the Jacobian satisfy $Re(\lambda_i) < 0$.

Lemma 2.1 [10]: If the origin of the linearized state equation is a stable node with distinct eigenvalues, a stable focus, or a saddle point, then, in a small neighborhood of the equilibrium point, the trajectories of the nonlinear state equation will behave like a stable node, a stable focus, or a saddle point, respectively.

The perturbed system has a stable equilibrium point at the origin, which is the desired operating point of the machine tool. Also, trajectories starting out in a small neighborhood of the origin will asymptotically converge to the origin. To obtain a global overview

of the system behavior, phase portraits are constructed. Figures 2 and 3 illustrate the system behavior for two different design specifications. While Figure 2 is globally stable, Figure 3 is clearly not and there exists a region of low initial forces where the system is unstable. It is desirable to be able to predict the region of attraction R_a defined as the set of all initial conditions whose trajectories converge to the stable equilibrium (origin) asymptotically as time tends to infinity.

In addition to the equilibrium discussed above, other equilibria may exist which cannot be computed analytically. However, the equilibrium points can be computed graphically by plotting equations (17a) and (17b) with the derivatives set to zero. The intersection points of the two curves are the system equilibriums. The equilibriums for the two cases corresponding to the phase plots in Figures 2 and 3 are plotted in Figures 4 and 5, respectively. The second case clearly has two equilibriums, one of which is the desired operating point. When the system is linearized about the other equilibrium point, the eigenvalues of the Jacobian of the closed–loop system are found to be unstable. From Theorem 2, this is an unstable equilibrium point.

Theorem 3 [10]: If the origin is an asymptotically stable equilibrium point for an autonomous nonlinear system, then its region of attraction R_a is an open connected, invariant set. Moreover, the boundary of R_a is formed by its trajectories.

Lemma 3.1 [11]: The boundary R_a is formed by whole trajectories and thus, as a consequence, the following holds true for $n = 2$. If R_a is bounded, its boundary is formed by either a limit cycle or a phase polygon (with unstable equilibrium points) or a closed curve of critical points.

The unstable equilibrium point lies on the stability boundary as expected by lemma 3.1. Moreover, the boundary of R_a can be obtained graphically by starting off at initial conditions close to the unstable equilibrium and developing a reverse trajectory [11]. This is illustrated in Figure 6 and the boundary obtained by this method exactly agrees with the phase portrait of Figure 3. The reverse trajectory is obtained by backward integration of the nonlinear system given by equation (16), i.e., by changing the sign of the right hand side of the expression. Also, it is observed that as the desired closed–loop poles are chosen further away from the open–loop poles, this unstable equilibrium point moves further away. This results in an increase in the region of instability.

The presence of a single stable equilibrium point is globally attractive since all trajectories converge to the only equilibrium in the state plane. The idea used in this paper to achieve global stability is to select the controller gains such that the unstable equilibrium lies outside the machine tool operation space (i.e., positive forces). The control law in equation (9) can be expressed as

$$\Delta f_{c_i} = -h_i\left(V_1\Delta F_1 + V_2\Delta F_2\right) \qquad i=1,2 \tag{18}$$

In terms of the actual feeds, the control law is

$$f_{c_i} = f_{n_i} - h_i\left[V_1\left(F_1 - F_{r_1}\right) + V_2\left(F_2 - F_{r_2}\right)\right] \qquad i=1,2 \tag{19}$$

With saturation limits the control law can be written as

$$f_{c_i} = \begin{cases} 0 & if \quad f_{c_i} < 0 \\ f_{n_i} - h_i\left(V_1\Delta F_1 + V_2\Delta F_2\right) & if \quad 0 \le f_{c_i} \le f_{\max} \\ f_{\max} & if \quad f_{c_i} > f_{\max} \end{cases} \qquad i=1,2 \tag{20}$$

Figure 7 graphically provides the lower saturation limits for design time constants corresponding to those of Figure 5. The saturation boundaries are obtained by calculating forces where the control law yields a feed of zero, i.e. by solving the equation

$$f_{n_i} + h_i\left(V_1F_{r_1} + V_2F_{r_2}\right) - h_i\left(V_1F_1 + V_2F_2\right) = 0 \qquad i=1,2 \tag{21}$$

In the case discussed above, saturation of the second feed interrupts the controller function at low initial forces. Further, it is seen that the slope of the saturation boundary is exactly the same as the stability boundary. It can be inferred that the saturation causes the instability. Also, in simulations it is the second force that goes unstable further reinforcing the direct relationship between saturation and the region of instability. The slopes of the saturation lines are given by

$$-\frac{h_iV_1}{h_iV_2} = -\frac{V_1}{V_2} < 0 \qquad i=1,2 \tag{22}$$

The slopes are negative meaning that if the gains are chosen such that the saturation boundaries pass through the origin or are below it, the entire saturation line will never occupy the first quadrant, which is the space of the machine tool operation. Thus, global asymptotic stability in the region of interest (i.e., for positive machining forces) is obtained by picking the gains such that

$$h_i \ge -\frac{f_{n_i}}{V_1F_{r_1} + V_2F_{r_2}} = -\frac{f_{n_i}}{P_{\max}} \qquad i=1,2 \tag{23}$$

The inequality of equation (23) provides sufficient conditions for global stability and is validated via phase portraits and simulations results.

The global stability of the parallel machining system evident in the phase portraits and by simulations is rigorously proved using the method of Lyapunov. The following scalar quadratic Lyapunov function is chosen

$$V = \frac{1}{2}\left(\Delta F_1^2 + \Delta F_2^2\right) \tag{24}$$

The function is clearly positive definite and is zero at the origin. Global stability can be proven if it can be shown that the time derivative of the Lyapunov function is negative definite. The derivative is obtained by using equations (16) and (24).

$$\dot V = \left[-\frac{\Delta F_1^2}{\tau_1} - \frac{\Delta F_1F_{r_1}}{\tau_1} + \frac{\bar K_1\Delta F_1}{\tau_1}\left[-h_1V_1\Delta F_1 - h_1V_2\Delta F_2 + f_{n_1}\right]^{\alpha_1}\right] + \left[-\frac{\Delta F_2^2}{\tau_2} - \frac{\Delta F_2F_{r_2}}{\tau_2} + \frac{\bar K_2\Delta F_2}{\tau_2}\left[-h_2V_1\Delta F_1 - h_2V_2\Delta F_2 + f_{n_2}\right]^{\alpha_2}\right] \tag{25}$$

The gains h_i (i=1,2) obtained from the equality of equation (23) are used in equation (25) to yield

$$\dot V = \frac{-\Delta F_1^2}{\tau_1} - \frac{\Delta F_1F_{r_1}}{\tau_1} + \frac{\Delta F_1\bar K_1}{\tau_1}\left[\overbrace{f_{n_1}\left\{1 + \frac{\overbrace{V_1\Delta F_1 + V_2\Delta F_2}^{T}}{V_1F_{r_1} + V_2F_{r_2}}\right\}}^{S_1}\right]^{\alpha_1} + \frac{-\Delta F_2^2}{\tau_2} - \frac{\Delta F_2F_{r_2}}{\tau_2} + \frac{\Delta F_2\bar K_2}{\tau_2}\left[\overbrace{f_{n_2}\left\{1 + \frac{\overbrace{V_1\Delta F_1 + V_2\Delta F_2}^{T}}{V_1F_{r_1} + V_2F_{r_2}}\right\}}^{S_2}\right]^{\alpha_2} \tag{26}$$

It is evident from equation (26) that the derivative of the Lyapunov function is zero at the origin. The function is analyzed for cases when the states are non–zero and proved to be negative

definite. The saturation constraints in equation (20) are used in the analysis. There are four possible cases.

Case I: $\Delta F_1 \geq 0$ and $\Delta F_2 \geq 0$

The term T of equation (26) is positive and, thus, $S_1 > f_{n_1}$ and $S_2 > f_{n_2}$. Therefore,

$$\dot{V} = \frac{-\Delta F_1^2}{\tau_1} \overbrace{-\frac{\Delta F_1 F_{r_1}}{\tau_1}}^{-ve} + \overbrace{\frac{\Delta F_1 \bar{K}_1}{\tau_1}\left[f_{n_1}\left\{1+\frac{V_1\Delta F_1 + V_2\Delta F_2}{V_1F_{r_1}+V_2F_{r_2}}\right\}\right]^{\alpha_1}}^{+ve} + (27)$$

$$\frac{-\Delta F_2^2}{\tau_2} \overbrace{-\frac{\Delta F_2 F_{r_2}}{\tau_2}}^{-ve} + \overbrace{\frac{\Delta F_2 \bar{K}_2}{\tau_2}\left[f_{n_2}\left\{1+\frac{V_1\Delta F_1 + V_2\Delta F_2}{V_1F_{r_1}+V_2F_{r_2}}\right\}\right]^{\alpha_2}}^{+ve}$$

The parameters α_i (i = 1,2) are between zero and one. The worst–case scenario for the derivative of the Lyapunov equation being negative is when the positive terms are maximum (i.e., $\alpha_1 = \alpha_2 = 1$). Equation (27) simplifies to

$$\dot{V} = \frac{-\Delta F_1^2}{2\tau_1} + \frac{-\Delta F_2^2}{2\tau_2} + \frac{V_1\Delta F_1\Delta F_2 F_{r_2}}{\tau_2\left(V_1F_{r_1}+V_2F_{r_2}\right)} + \frac{V_2\Delta F_1\Delta F_2 F_{r_1}}{\tau_1\left(V_1F_{r_1}+V_2F_{r_2}\right)} \quad (28)$$

The first and second partial derivatives of $\dot{V}$ with respect to ΔF_1 and ΔF_2, respectively, are

$$\begin{aligned} \frac{\partial(\dot{V})}{\partial(\Delta F_1)} &= -2\tau_2\Delta F_1 + \left(2\tau_1V_1F_{r_2} + 2\tau_2V_2F_{r_1}\right)\Delta F_2 = 0 \\ \frac{\partial(\dot{V})}{\partial(\Delta F_2)} &= -2\tau_1\Delta F_2 + \left(2\tau_1V_1F_{r_2} + 2\tau_2V_2F_{r_1}\right)\Delta F_1 = 0 \\ \frac{\partial^2(\dot{V})}{\partial(\Delta F_1)^2} &= -2\tau_2 < 0 \qquad \frac{\partial^2(\dot{V})}{\partial(\Delta F_1)^2} = -2\tau_1 < 0 \end{aligned} \quad (29)$$

The only solution to the first two equations of equation (29) is $\Delta F_1 = \Delta F_2 = 0$ and this solution is a maximum. Thus, the term $\dot{V}$ is negative in the first quadrant except at the origin.

Case II: $\Delta F_1 \leq 0$ and $\Delta F_2 \leq 0$

The term T of equation (26) is now negative and, thus, $S_1 < f_{n_1}$ and $S_2 < f_{n_2}$. This case is similar to *Case I* except that the signs of the non–square terms are reserved.

$$\dot{V} = -\frac{\Delta F_1^2}{\tau_1} - \frac{\Delta F_1 F_{r_1}}{\tau_1} + \frac{\Delta F_1 F_{r_1}}{\tau_1}\left[1+\frac{V_1\Delta F_1 + V_2\Delta F_2}{V_1F_{r_1}+V_2F_{r_2}}\right]^{\alpha_1} + (30)$$

$$-\frac{\Delta F_2^2}{\tau_2} - \frac{\Delta F_2 F_{r_2}}{\tau_2} + \frac{\Delta F_2 F_{r_2}}{\tau_2}\left[1+\frac{V_1\Delta F_1 + V_2\Delta F_2}{V_1F_{r_1}+V_2F_{r_2}}\right]^{\alpha_2}$$

The worst–case scenario for the derivative of the Lyapunov equation being negative is when the negative terms are minimum (i.e., $\alpha_1 = \alpha_2 = 1$). In this case, equation (30) is

$$\dot{V} = -\frac{\Delta F_1^2}{2\tau_1} - \frac{\Delta F_2^2}{2\tau_2} + \frac{V_1\Delta F_1\Delta F_2 F_{r_2}}{\tau_2(V_1F_{r_1}+V_2F_{r_2})} + \frac{V_2\Delta F_1\Delta F_2 F_{r_1}}{\tau_1(V_1F_{r_1}+V_2F_{r_2})} \quad (31)$$

Computing the maximum along the same lines as in the previous case, it is found that the maximum is at the origin of the perturbed force state space. At the origin, $\dot{V}$ is zero. This clearly implies that everywhere else in the third quadrant the derivative of the Lyapunov function is negative.

Case III: $\Delta F_1 > 0$ and $\Delta F_2 < 0$

This case represents the fourth quadrant of the state space and can be further divided into two cases: one when $|V_1\Delta F_1| > |V_2\Delta F_2|$ and one when $|V_1\Delta F_1| < |V_2\Delta F_2|$. In the first case, the term T in equation (26) is positive and, thus, $S_1 > f_{n_1}$ and $S_2 > f_{n_2}$. Therefore, it follows that

$$\left|\frac{\Delta F_2\bar{K}_2}{\tau_2}\left[f_{n_2}\left\{1+\frac{V_1\Delta F_1 + V_2\Delta F_2}{V_1F_{r_1}+V_2F_{r_2}}\right\}\right]^{\alpha_2}\right| > \left|\frac{\Delta F_2 F_{r_2}}{\tau_2}\right| \quad (32)$$

and, consequently, implies that the last two terms of equation (26) taken together are negative. The rest of the derivative is denoted by J and given is by

$$J = -\frac{\Delta F_1^2}{\tau_1} - \frac{\Delta F_2^2}{\tau_2} - \frac{\Delta F_1 F_{r_1}}{\tau_1} + \frac{\Delta F_1 F_{r_1}}{\tau_1}\left[\underbrace{1+\frac{V_1\Delta F_1 + V_2\Delta F_2}{V_1F_{r_1}+V_2F_{r_2}}}_{Z}\right]^{\alpha_1} \quad (33)$$

where $Z > 1$. The worst–case scenario corresponds to $\alpha_1 = 1$. The negative definiteness is thus proved only for this worst case.

$$J = -\frac{\Delta F_1^2}{2\tau_1} - \frac{\Delta F_2^2}{\tau_2} + \frac{\Delta F_1\Delta F_2 V_2 F_{r_1}}{\tau_1\left(V_1F_{r_1}+V_2F_{r_2}\right)} < 0 \quad (34)$$

All of the terms in equation (34) are negative. For the case when $|V_1\Delta F_1| < |V_2\Delta F_2|$, the term T in equation (26) is negative and, thus, $S_1 < f_{n_1}$ and $S_2 < f_{n_2}$. It follows that

$$\left|\frac{\Delta F_1\bar{K}_1}{\tau_1}\left[f_{n_1}\left\{1+\frac{V_1\Delta F_1 + V_2\Delta F_2}{V_1F_{r_1}+V_2F_{r_2}}\right\}\right]^{\alpha_1}\right| < \left|\frac{\Delta F_1 F_{r_1}}{\tau_1}\right| \quad (35)$$

and, consequently, implies that the second and third terms of equation (26) added together are negative. The rest of the derivative is denoted by L and given by

$$L = -\frac{\Delta F_1^2}{\tau_1} - \frac{\Delta F_2^2}{\tau_2} + \frac{\Delta F_2 F_{r_2}}{\tau_2}\left[\underbrace{1+\frac{V_1\Delta F_1 + V_2\Delta F_2}{V_1F_{r_1}+V_2F_{r_2}}}_{Z}\right]^{\alpha_2} - \frac{\Delta F_2 F_{r_2}}{\tau_2} \quad (36)$$

where $Z < 1$. The worst–case scenario corresponds to $\alpha_1 = 1$. The negative definiteness is thus proved only for this worst case.

$$L = -\frac{\Delta F_1^2}{2\tau_1} - \frac{\Delta F_2^2}{\tau_2} + \frac{\Delta F_1\Delta F_2 V_1 F_{r_2}}{\tau_2\left(V_1F_{r_1}+V_2F_{r_2}\right)} < 0 \quad (37)$$

The parameter L is clearly negative since all the three terms of equation (37) are negative. This proves the negative definiteness of the derivative of the Lyapunov function for this case.

Case IV: $\Delta F_1 < 0$ and $\Delta F_2 > 0$

This case is along the same lines as *Case III* and, thus, is not illustrated in this paper. A similar derivation shows that the function is negative at all points. Thus global stability is achieved in the second quadrant.

Clearly, it can be concluded that the time derivative of the Lyapunov is negative definite in the region of interest and this implies global asymptotic stability of the system. Thus, a rigorous mathematical stability analysis is established.

SUMMARY AND CONCLUSIONS – A model based machining force control system is presented for a parallel turning operation using output feedback control. This approach incorporates a mathematical model for the process coupled with first order servo dynamics. The model is developed from empirical cutting force

data and includes basic machining nonlinearities. The nonlinear model is linearized to compute the output feedback controller gains. The controller design algorithm is given in three steps and is simple to implement. Equilibrium analysis and effects of saturation are used to analyze system behavior. It is found that the system is unstable when the initial forces are close to the origin of the perturbed force system. An unstable equilibrium lying on the saturation boundary is found to be the cause for this type of behavior. Sufficient conditions for global stability are developed by obtaining mathematical constraints that ensure that the unstable equilibrium and saturation boundary are outside the global operation space of the machine tool. Phase portraits of the system prove the analysis. The reverse trajectory method is employed to show the numerical construction of the stability boundary, which closely agree with the simulation results. Further, global stability is proved for the closed loop system using the method of Lyapunov.

NOMENCLATURE

d_i (i = 1,2):	depth of cut (*mm*) of i^{th} tool
f_{c_i} (i = 1,2):	commanded feed (*mm*) of i^{th} tool
f_i (i = 1,2):	actual feed (*mm*) of i^{th} tool
f_{n_i} (i = 1,2):	nominal feed (*mm*) of i^{th} tool
F_i (i = 1,2):	cutting force (*kN*) of i^{th} tool
F_{r_i} (i = 1,2):	reference cutting force (*kN*) of i^{th} tool
Δf_{c_i} (i = 1,2):	perturbed commanded feed (*mm*) of i^{th} tool
ΔF_i (i = 1,2):	perturbed cutting force (*kN*) of i^{th} tool
$H = (h_1, h_2)^T$:	gain vector used in feedback control law
K:	full state feedback gain matrix
K_i (i = 1,2):	cutting coefficient (kN/mm^2) of i^{th} tool
$\bar{K}_i$ (i = 1,2):	static gain of i^{th} tool (kN/mm^2)
$\bar{K}_{ia}$ (i = 1,2):	linearized cutting coefficient of i^{th} tool
m:	number of outputs
m_i (i = 1,2):	desired time constants (*s*)
n:	number of states
N_S:	spindle speed (*rpm*)
p:	number of inputs
P:	spindle power (*kW*)
P_{max}:	maximum spindle power (*kW*)
ΔP:	perturbed spindle power (*kW*)
R_a:	region of attraction
V:	Lyapunov function
V_i (i = 1,2):	cutting velocity (*km/min*) of i^{th} tool
α_i (i = 1,2):	feed–force exponent of i^{th} force process
β_i (i = 1,2):	depth of cut–force exponent of i^{th} force process
γ_i (i = 1,2):	cutting velocity–force exponent of i^{th} force process
τ_i (i = 1,2):	open–loop time constant (*s*) of i^{th} servo system

REFERENCES

[1] Ulsoy, A.G., Koren, Y., and Rasmussen, F., 1983, "Principle Developments in the Adaptive Control of Machine Tools," *ASME Journal of Dynamic Systems, Measurement, and Control*, Vol. 105, No. 2, pp. 107–112.

[2] Landers, R.G. and Ulsoy, A.G., 2000, "Model–Based Machining Force Control," *ASME Journal of Dynamics Systems, Measurement, and Control*, Vol. 122, No. 3, pp. 521–527.

[3] Rober, S.J., Shin, Y.C., and Nwokah, O.D.I., 1997, "A Digital Robust Controller for Cutting Force Control in the End Milling Process," *ASME Journal of Dynamic Systems, Measurement, and Control*, Vol. 119, No. 2, pp. 146–152.

[4] Levin, J.B. and Dutta, D., 1996, "PMPS: A Prototype CAPP System for Parallel Machining," *Journal of Manufacturing Science and Engineering*, Vol. 118, No. 3, pp. 406–414.

[5] Yip–Hoi, D. and Dutta, D., 1995, "Data Extraction from Geometric Models for Process Planning for Parallel Machines," *Journal of Manufacturing Systems*, Vol. 14, No. 5, pp. 307–318.

[6] Kimura, H., 1975, "Pole Assignment by Gain Output Feedback," *IEEE Transactions on Automatic Control*, Vol. AC–20, No. 4, pp. 509–516.

[7] Friedland, B., 1986, *Control System Design: An Introduction to State Space Methods*, McGraw–Hill, Inc., New York.

[8] Sinha, P.K., 1984, *Multivariable Control: An Introduction*, Marcel Dekker, Inc., New York.

[9] Sandoval, J.E., Landers, R.G., and Ulsoy, A.G., 2001, "Reconfigurable CNC Lathe Simulation System," *ERC/RMS Technical Report*, University of Michigan, Ann Arbor, Michigan.

[10] Khalil, H., 1996, *Nonlinear Systems*, Second Edition, Prentice Hall, Upper Saddle River, New Jersey.

[11] Genesio, R., Tartaglia, M., and Vicino, A., 1985, "On the Estimation of Asymptotic Stability Regions: State of the Art and New Proposals," *IEEE Transactions on Automatic Control*, Vol. AC–30, No. 8, pp. 747–755.

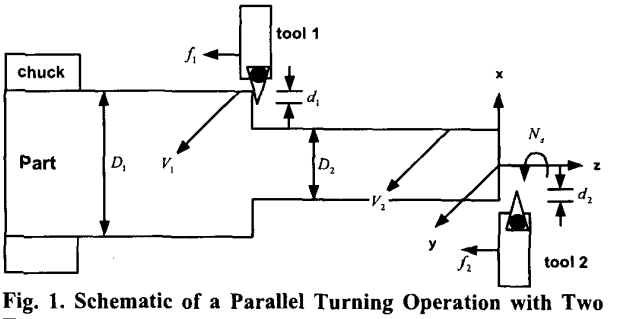

Fig. 1. Schematic of a Parallel Turning Operation with Two Tools.

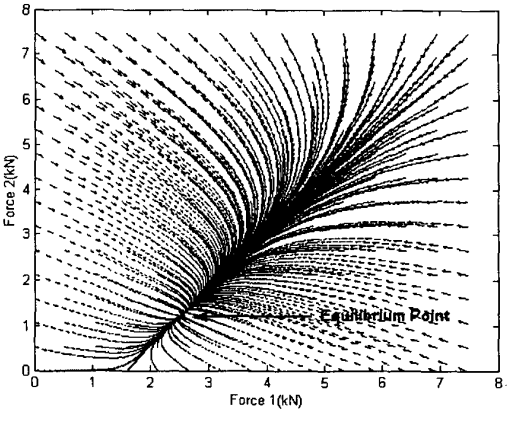

Fig. 4. Phase Plot: $m_1 = 0.5$ *s*, $m_2 = 0.49$ *s*, and Controller Gains Given by Equation (15).

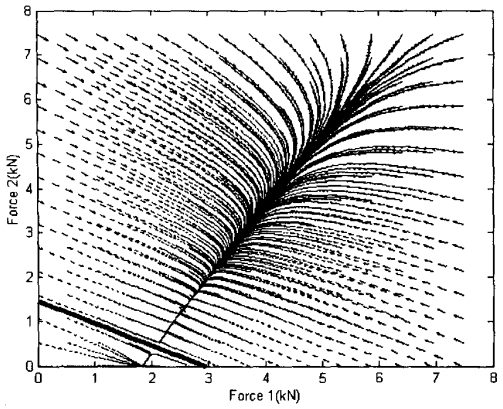

Fig. 5. Phase Plot: $m_1 = 1.5$ *s*, $m_2 = 1.49$ *s*, and Controller Gains Given by Equation (15). Stability Boundary Given by Thick Line.

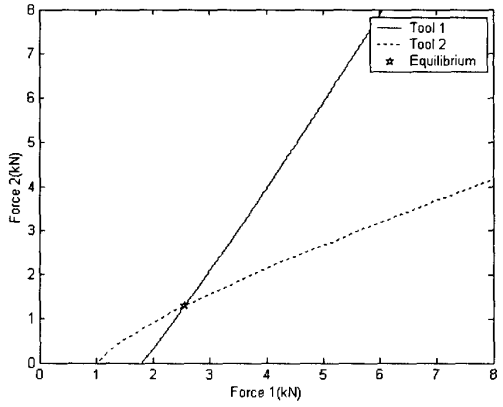

Fig. 6. Plot of Equation (17a) = 0 (solid line) and Equation (17b) = 0 (dotted line). $m_1 = 0.5$ *s*, $m_2 = 0.49$ *s*, and Controller Gains Given by Equation (15).

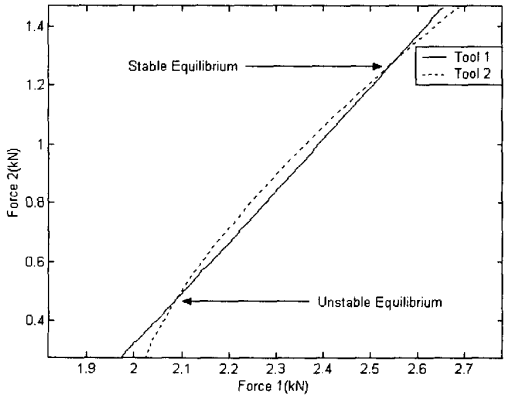

Fig. 7. Plot of Equation (17a) = 0 (solid line) and Equation (17b) = 0 (dotted line). $m_1 = 1.5$ *s*, $m_2 = 1.49$ *s*, and Controller Gains Given by Equation (15).

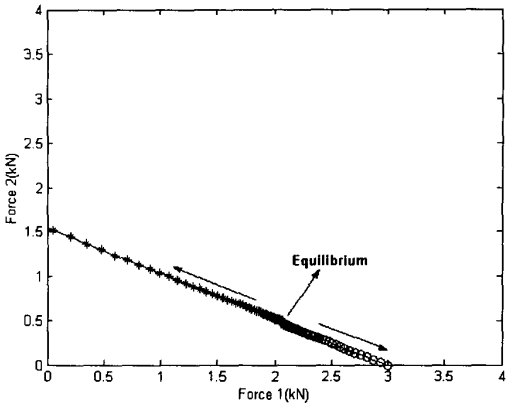

Fig. 8. R_a by Reverse Trajectory. $m_1 = 1.5$ *s*, $m_2 = 1.49$ *s*, and Controller Gains Given by Equation (15).

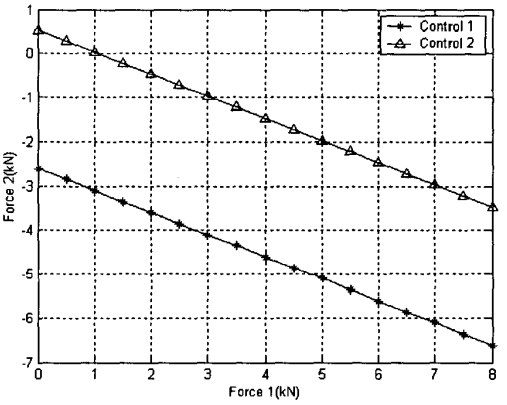

Fig. 9. Plot of Equation (21) = 0 for $i = 1$ (stars) and $i = 2$ (triangles) Illustrating Control Saturation Boundaries for the First and Second Tool, Respectively. $m_1 = 1.5$ *s*, $m_2 = 1.49$ *s*, and Controller Gains Given by Equation (15).

Table 1. Parameters used in Simulation Studies.

Parameter	Tool 1	Tool 2	Unit
f_n	0.528	0.875	*mm*
α	0.89	0.89	–
β	0.87	0.87	–
γ	–0.27	–0.27	–
K	1.17	1.17	kN/mm^2
D	0.05	0.10	*m*
d	0.003	0.001	*m*
τ	0.05	0.049	*s*
P	20		*kW*
N_s	1500		*rpm*